Demonstration of Super-Resolution for Tomographic SAR Imaging in Urban Environment

Xiao Xiang Zhu, *Member, IEEE*, and Richard Bamler, *Fellow, IEEE*

***Abstract*—Tomographic synthetic aperture radar (SAR) inversion, including SAR tomography and differential SAR tomography, is essentially a spectral analysis problem. The resolution in the elevation direction depends on the elevation aperture size, i.e., on the spread of orbit tracks. Since the orbits of modern meter-resolution spaceborne SAR systems, such as TerraSAR-X, are tightly controlled, the tomographic elevation resolution is at least an order of magnitude lower than in range and azimuth. Hence, super-resolution (SR) reconstruction algorithms are desired. Considering the sparsity of the signal in elevation, a compressive sensing based super-resolving algorithm, named "Scale-down by L_1 norm Minimization, Model selection, and Estimation Reconstruction" (SL1MMER, pronounced "slimmer"), was proposed by the authors in a previous paper. The ultimate bounds of the technique on localization accuracy and SR power were investigated. In this paper, the essential role of SR for layover separation in urban infrastructure monitoring is indicated by geometric and statistical analysis. It is shown that double scatterers with small elevation distances are more frequent than those with large elevation distances. Furthermore, the SR capability of SL1MMER is demonstrated using TerraSAR-X real data examples. For a high rise building complex, the percentage of detected double scatterers is almost doubled compared to classical linear estimators. Among them, half of the detected double scatterer pairs have elevation distances smaller than the Rayleigh elevation resolution. This confirms the importance of SR for this type of applications.**

***Index Terms*—Compressive sensing, SL1MMER, sparse reconstruction, super-resolution, synthetic aperture radar, TerraSAR-X, tomographic SAR inversion.**

I. Introduction

A SINGLE synthetic aperture radar (SAR) image can only provide cartographic information in the two native coordinates "azimuth" (x) and "range" (r). Tomographic SAR Inversion, including SAR tomography (TomoSAR) [1]–[3] and differential SAR tomography (D-TomoSAR) [4]–[6], aims at retrieving the 3-D position, i.e., including the "elevation" (s) coordinate, as well as motion information of the scattering objects by exploiting stacks of complex-valued SAR images with diversity in space and time.

In urban environment, the most important task is to resolve layover, i.e., to detect multiple discrete scatterers inside a pixel [7]. Here, the term "pixel" means an azimuth-range pixel, and the term "multiple scatterers" means the presence of several scattering objects in the same pixel, e.g., from the building facade and the ground, but at different elevation positions. For this purpose, TomoSAR has been applied to C-band European Remote Sensing (ERS) satellite data of extended scenes over the Bay of Naples in [8], to TerraSAR-X data over downtown Las Vegas in [9] and to L-band airborne SAR data acquired by the DLR's Experimental SAR (E-SAR) system over the city of Dresden in Germany in [10], [11]. In [12], single and double scatterer cases were separated at the same test site as in [8]. Another attempt to separate layover scatterers can be found in [13] which extended the concept of permanent scatterers to two scatterers inside a pixel.

Resolving discrete scatterers with possible motion is also referred to as D-TomoSAR or 4-D SAR focusing. The goal is not only to separate targets interfering in the same azimuth-range pixel, but also to estimate their possible relative motion. It exploits the strength of both TomoSAR (3-D SAR imaging) and PSI (long-term motion monitoring). This concept was proposed in [4], applied to ERS real data in [5], and applied to TerraSAR-X data in [14]. The extraction of time series of displacement for single and double interfering scatterers based on the so-called velocity spectrum was presented in [5]. The generalized "time warp" method is proposed in [15] to estimate multicomponent nonlinear motion.

Tomographic SAR inversion is essentially a spectral estimation problem. The Rayleigh elevation resolution is given by [14]

$$\rho_s = \frac{\lambda r}{2\Delta b} \tag{1}$$

where λ is the wavelength and Δb is the elevation aperture size, i.e., the spread of orbit tracks perpendicular to the line-of-sight direction. Due to the tight orbital tube of modern SAR satellites required by differential interferometric SAR (D-InSAR) applications, the elevation aperture is small and, as a consequence, the Rayleigh resolution in elevation is typically about 50 times worse than in azimuth or range. For example, for TerraSAR-X high-resolution spotlight images, the range and azimuth resolutions are 0.6 m and 1.1 m, respectively, while $\rho_s \simeq 30 \sim 50$ m.

Linear reconstruction methods are only able to resolve two scatterers with an elevation distance $\delta s \gtrsim \rho_s$. Parametric methods or nonparametric methods that favor sparse solutions [16], [17] promise to give super-resolution (SR). In [18], the authors proposed a super-resolving algorithm based on $L_1 - L_2$ norm minimization, named "Scale-down by L_1 norm Minimization, Model selection, and Estimation Reconstruction" (SL1MMER,

Manuscript received September 16, 2011; accepted November 20, 2011. Date of publication December 27, 2011; date of current version July 18, 2012. This work was supported by the International Graduate School of Science and Engineering, Technische Universität München (TUM) and German Research Foundation (DFG).

The authors are with the Remote Sensing Technology Institute (IMF), German Aerospace Center (DLR), Oberpfaffenhofen, 82234 Wessling, Germany and also with the Lehrstuhl für Methodik der Fernerkundung, Technische Universität München (TUM), 80333 München, Germany (e-mail: xiao.zhu@dlr.de; richard.bamler@dlr.de).

Digital Object Identifier 10.1109/TGRS.2011.2177843

pronounced "slimmer"). In [19], we investigated the SR power and estimation accuracy of this algorithm for separating two closely spaced scatterers with $\delta s < \rho_s$. The SR problem was treated as a detection problem. The elevation resolution $\rho_{50\%}$ was defined as the minimum distance between two scatterers that are separable at a probability of detection of 50%. The SR factor $\kappa_{50\%}$ was therefore defined by

$$\kappa_{50\%} = \frac{\rho_s}{\rho_{50\%}}. \tag{2}$$

In [19] it was pointed out that

- The SR factor of SL1MMER depends asymptotically on the product of the number of acquisitions N and signal-to-noise ratio (SNR).
- Irregular aperture sampling does not have a large impact on SR.
- The detection rate varies dramatically with the phase difference between the two scatterers $\Delta\varphi$.
- Within the interesting parameter range of TomoSAR, i.e., $SNR = 0 \sim 10$ dB, $N = 10 \sim 100$, the SR factor of the algorithm (averaged over all possible phase difference of the two scatterers) is in the order $1.5 \sim 25$.

In [19], the SR capability of the proposed SL1MMER algorithm was illustrated by examples using simulated data. Further practical super-resolving examples by reconstructing several selected pixels were provided in [18]. So far, no substantial real data example has been presented. In this paper, the relevance of SR for urban infrastructure monitoring is pointed out. Furthermore, a practical demonstration of the SR of SL1MMER for SAR tomographic reconstruction is presented using a stack of TerraSAR-X high-resolution spotlight data.

II. Role of Super-Resolution for Urban Infrastructure Monitoring

The layover phenomenon in a SAR image of an urban area is mainly caused by the following two scenarios:

- *Buildings with different heights in layover with the ground*: As sketched in Fig. 1(a), the layovers caused by the taller building and the lower building both contain areas with smaller elevation distances. However, only the layover areas of the taller building exhibits larger elevation distances.
- *Taller building in layover with the ground and the roof of the lower building*: As sketched in Fig. 1(b), the layover of the taller building and lower building also leads to smaller elevation distances.

Both scenarios suggest that double scatterer pairs with smaller elevation distances will be more frequent than those with larger distances.

By assuming the layover phenomena are mainly caused by the simple scenario of Fig. 1(a), the probability density function $p(\delta s)$ of the elevation distance between two scatterers δs is given by

$$p(\delta s) = \int p(\delta s|h)p(h)dh. \tag{3}$$

where $p(h)$ is probability density function of the building height, while $p(\delta s|h)$ gives the conditional distribution for δs given h.

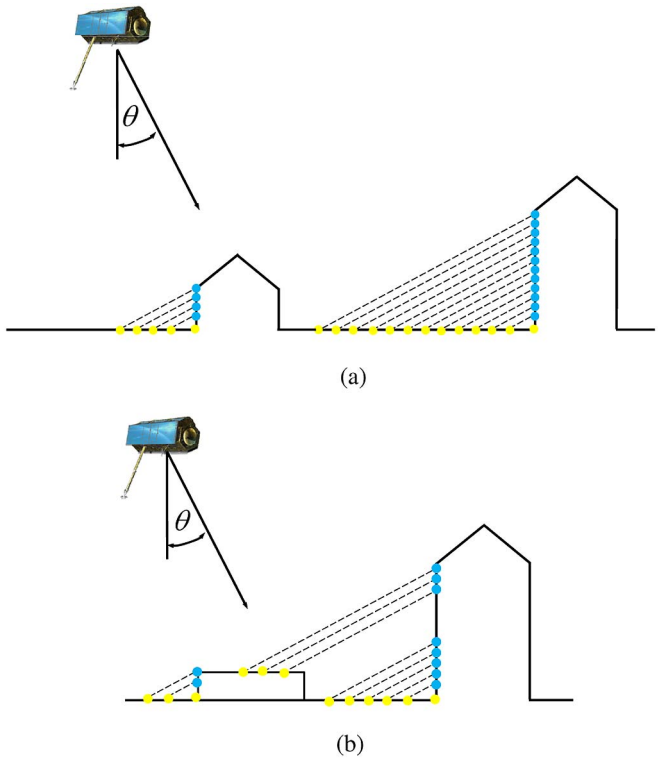

Fig. 1. Double scatterer pairs are more probable with small elevation distances. Typical scenarios of layover. (a) Buildings with different heights in layover with the ground. (b) Taller building in layover with the ground and the roof of the lower building.

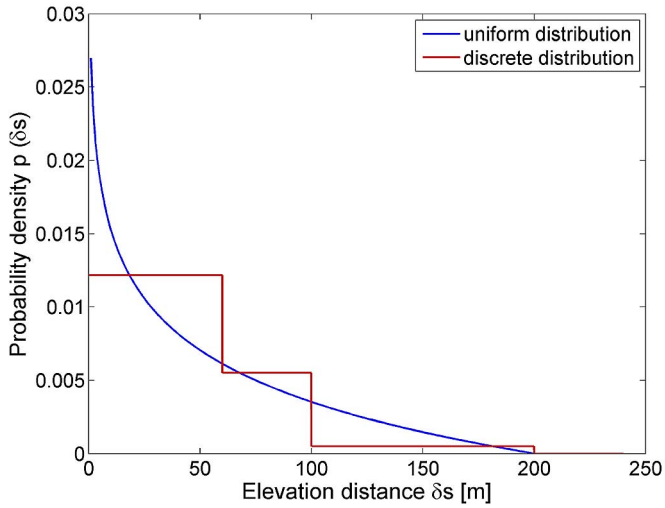

Fig. 2. Probability density function of the elevation distance between two scatterers in a layover area by assuming uniformly (blue) and discretely (red) distributed building heights.

Let us assume homogenous scattering properties of the ground and the facade. Then, for a given h, it is natural to assume that δs follows a uniform distribution

$$p(\delta s|h) = \begin{cases} \sin\theta/h, & 0 < \delta s \le h/\sin\theta \\ 0, & \text{else} \end{cases} \tag{4}$$

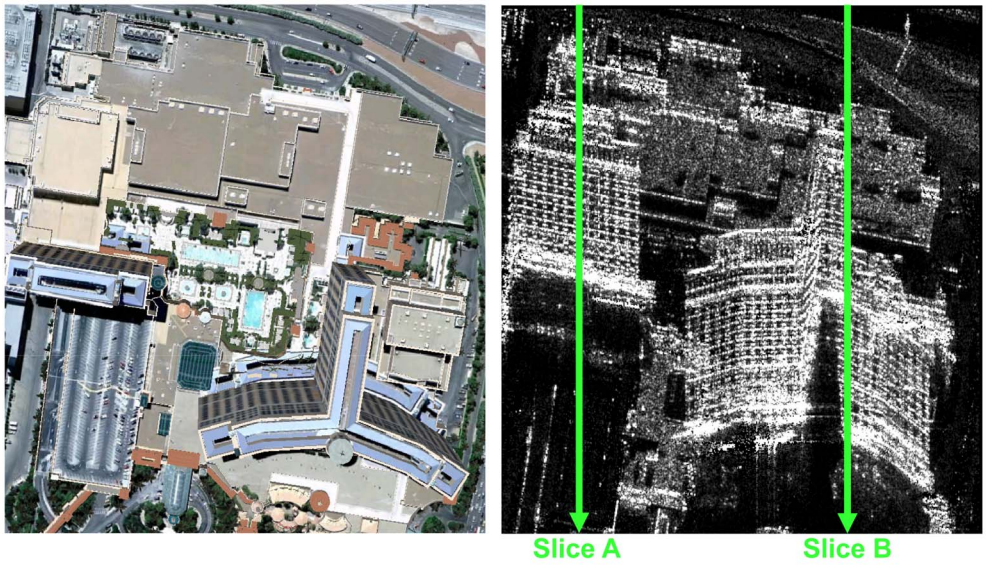

Fig. 3. Test building: Bellagio hotel. (a) Optical image (Copyright Google). (b) TerraSAR-X mean intensity map and the green arrows mark the analysis slice A and B shown in Fig. 10.

where θ is the incidence angle (see Fig. 1). Inserting (4) into (3), it yields

$$p(\delta s) = \int\limits_{h \geq \delta s \sin\theta} \frac{\sin\theta}{h} p(h) dh. \tag{5}$$

Two examples for height distributions are as follows.

- *Uniformly distributed building height*: If the heights of the buildings also follow a uniform distribution within the range between zero and maximum building height $h_{\max}$, i.e.,

$$p(h) = \begin{cases} 1/h_{\max} & 0 < h \leq h_{\max} \\ 0 & \text{else} \end{cases} \tag{6}$$

  the elevation distance between the double scatterer pairs should follow approximately a *logarithmic* law

$$p(\delta s) = \frac{\sin\theta}{h_{\max}} \left(\ln(h_{\max}) - \ln(\delta s \sin\theta) \right); \quad \text{for } \delta s = 0, \ldots, \frac{h_{\max}}{\sin\theta} \tag{7}$$

  $p(\delta s)$ with $h_{\max} = 100$ m and $\theta = 30$ degree is drawn in Fig. 2 (blue curve).
- *Discrete building height distribution*: In practice, restricted by the city planning policy, the building heights often only occupy several discrete numbers. Let us assume the buildings only have three heights with $p(h = 20\,\text{m}) = 0.4$, $p(h = 50\,\text{m}) = 0.5$, $p(h = 100\,\text{m}) = 0.1$, the corresponding $p(\delta s)$ obtained according to (5) with $\theta = 30$ degree is displayed in Fig. 2 (red curve).

From these purely geometric and simple statistical considerations, it is obvious that the majority of layover areas contain double scatterers with small elevation distances. Taking into account the poor elevation resolution caused by the tight orbit control of modern SAR sensors, SR is a very crucial requirement for very high resolution tomographic SAR inversion for urban infrastructure monitoring.

III. Practical Demonstration of the Super-Resolution of SL1MMER

In this section, we demonstrate that SR is possible with the proposed SL1MMER algorithm by providing real data examples.

A. Test Site

We work with TerraSAR-X high resolution spotlight data with a slant-range resolution of 0.6 m and an azimuth resolution of 1.1 m. The stack used in this paper consists of 30 images covering a time period of more than 1 year, from February 2008 to June 2009, over downtown Las Vegas. This stack has an elevation aperture size of about 269.5 m, i.e., the inherent elevation resolution is $\rho_s = 40.5$ m, i.e., approximately 20 m resolution in height with the elevation-to-height factor $\sin\theta$, where the incidence angle θ is 31.8° here.

The Las Vegas Bellagio hotel is chosen as a test building to demonstrate the SR power of SL1MMER since its surrounding infrastructure exhibits strong scatterers that compete with the reflections from the building facade. It is expected that the SR capability of the algorithm will be observed when reconstructing the layover area where the lower part of the building and the ground infrastructures are mapped together. Fig. 3(a) shows the optical view of the Bellagio hotel in Las Vegas with a height close to 125 m, corresponding to an elevation extent of 237 m. Fig. 3(b) is the corresponding TerraSAR-X mean intensity image. Compared to the optical image, noteworthy features of the SAR image are: 1) The folding of the building toward the sensor due to the layover phenomenon (the optic image and the TerraSAR image are cropped such that the base of the Bellagio hotel is almost horizontally aligned) and 2) Due to the weaker backscattering, ground infrastructure visible in the optical image is completely "hidden" by the strong returns from the building facade in the SAR image.

The goal is to separate the interfering layers associated with the ground infrastructure and the facade of the building and to reconstruct the 3-D shape and motion of the building.

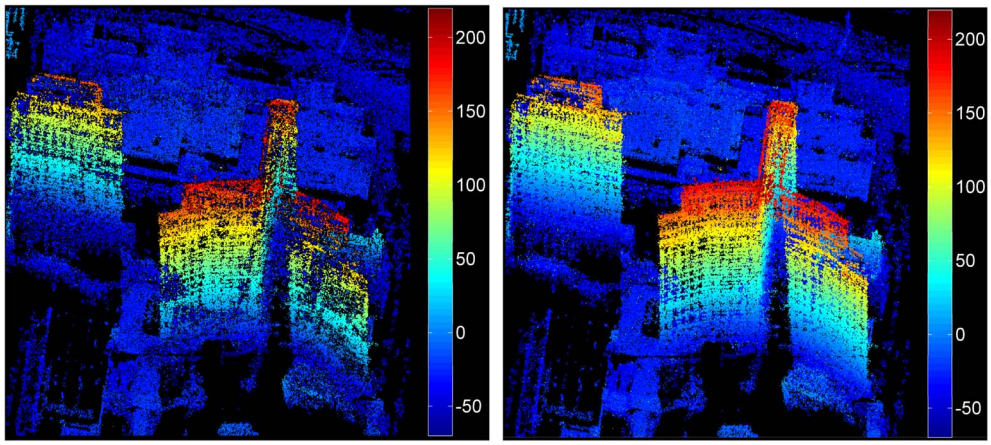

Fig. 4. Elevation estimates in meters. (Left) Detected single scatterers. (Right) Detected single and double scatterers (for double scatterers the higher one (facade) is displayed).

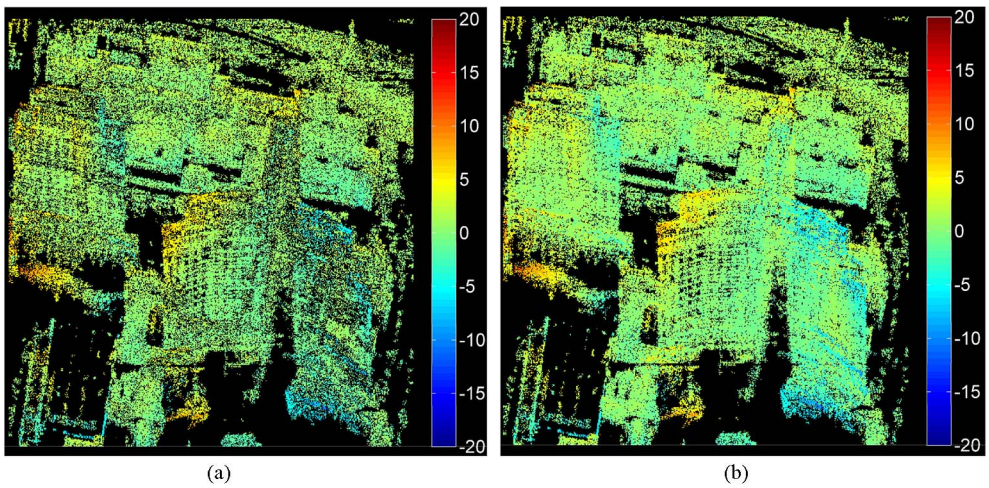

Fig. 5. Amplitude of seasonal motion estimates in millimeters. (Left) Detected single scatterers. (Right) Detected single and double scatterers (for double scatterers the higher one (facade) is displayed).

B. Experimental Results

The preprocessing including atmosphere phase screen correction is performed by the German Aerospace Center (DLR) PSI-GENESIS system on a persistent scatterer network of high-SNR pixels containing only single scatterers [20]. Within the acquisition period of this stack, no long-term motion has been observed in the test area, i.e., motion-induced phase is only caused by periodic thermal dilation. The D-TomoSAR system model with a time warp operation assuming a sinusoidal seasonal motion is used [15]. The SL1MMER algorithm with Bayesian information criterion [21] as the model selection scheme is applied to each pixel of the test area. The number of scatterers map, elevation, and amplitude of seasonal motion for each of the detected single and double scatterers are then obtained.

Fig. 4(a) presents the topography estimates, i.e., the estimated elevations, of the detected single scatterers. The fused topography estimates both with the detected single scatterers and the top layer of the detected double scatterers (blue points in Fig. 1) are shown in Fig. 4(b). The information increment contributed by layover separation is significant, and the high density of detected double scatterers completes the structures of individual high rise buildings.

The same plots as shown in Fig. 4 but with the estimated amplitude of the seasonal motion are exhibited in Fig. 5. The motion patterns are quite complex. This is due to the fact that thermal dilation of buildings depends on many effects, like environmental air temperature, current sun illumination, internal cooling or heating, and the location of the major construction elements with respect to the facade. In this case, the southern, sun illuminated, part (left) of the facades show stronger seasonal deformation, while the northern parts have even a negative amplitude, i.e., a phase reversal. The higher the building, the more pronounced the thermal effects are. Note that buildings with no internal heating or cooling and simpler construction exhibit a much more consistent relationship between seasonal dilation and height. See e.g., [22] where the Berlin Railway station is investigated. Since the goal is to demonstrate the SR of SL1MMER and the shape of the building can provide plausibility for the elevation estimates, the following discussion about the detected double scatterers will be focused on the elevation (rather than the motion) estimates.

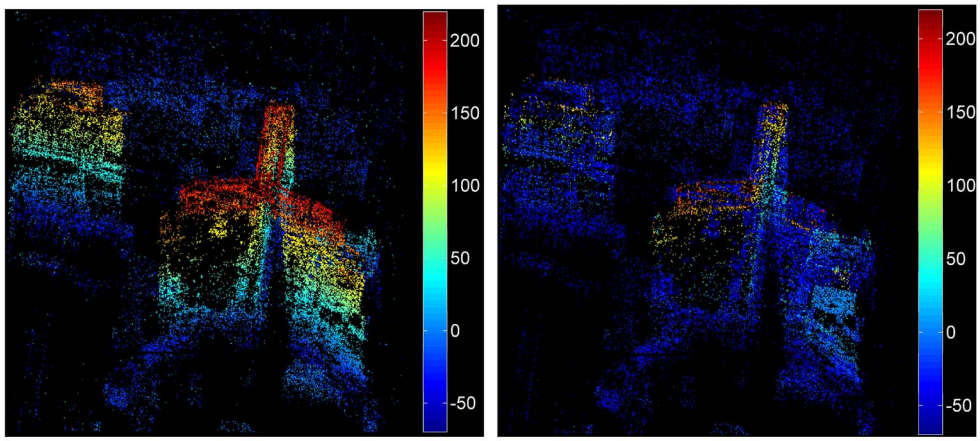

Fig. 6. Elevation estimates of the separated double scatterers. (a) Top layer, mostly caused by returns from building facade. (b) Ground layer, mostly caused by returns from ground structures.

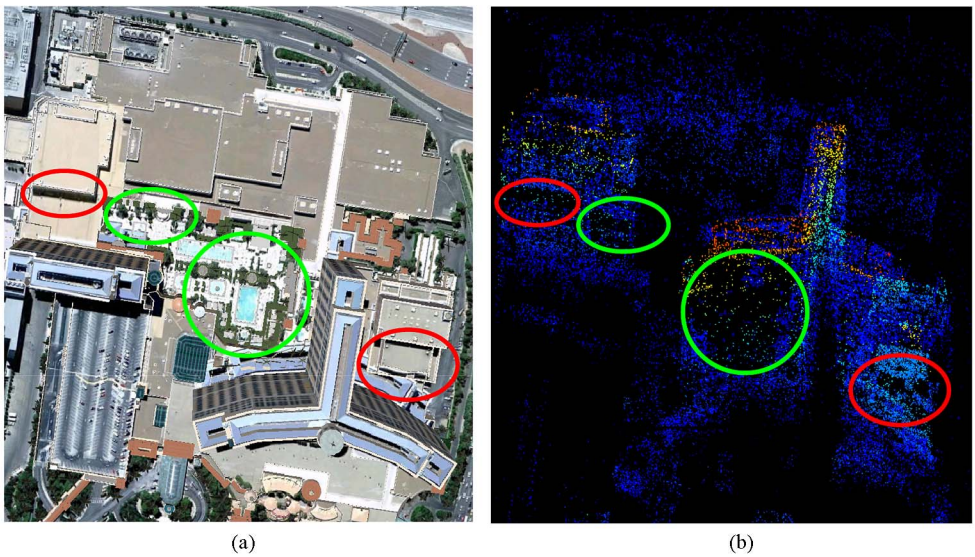

Fig. 7. Layovered ground infrastructure: Optical image (Copyright Google) versus reconstruction from layover separation obtained by SL1MMER. The red circles: shadowing areas; the green circle: vegetation areas. (a) Optical image (Copyright Google). (b) Layovered ground infrastructure reconstructed by SL1MMER (lower layer—one of the detected double scatterers).

Fig. 6 presents the elevation estimates of the two layers of the detected double scatterers, i.e., a top layer mostly caused by reflections from the facade of the high rise building and a ground layer caused by reflections from lower buildings and ground infrastructures (yellow points in Fig. 1). The gradation of elevation estimates on the top layer [see Fig. 6(a)] and the homogeneity on the ground layer [see Fig. 6(b)] suggest the correctness of the elevation estimation and the layover separation capability. It is interesting to observe that the full structure of the high rise building is almost captured even only with the detected double scatterers. In addition, hidden ground infrastructures are now "visible." In Fig. 7, the reconstructed elevation of the ground infrastructure [Fig. 7(b)] is interpreted with the assistance of the optical image [Fig. 7(a)].

- There are two blocks on the ground layer (left top and right bottom, respectively) that show brighter blue. This indicates higher topography at that area, and this is consistent with the 3-D building model provided by Google earth.
- Although most of the hidden ground infrastructure is retrieved, there are still some areas (e.g., the ones marked by circles) showing homogenous black color, i.e., no layovered coherent object on the ground layer. By comparison with the optical image, it can be easily found that the areas marked by red circles are shadowing areas that can also be seen in SAR image while the areas marked by green circles are vegetation areas, i.e., no coherent return. This fact confirms our estimates.
- Some pixels at the area near the top of the building have very large elevation estimates showing some regular structures even for the lower layer. It seems that both of the detected scatterers are located on the building facade or the building roof. This might be caused by the complicated structure on the top of the Bellagio hotel. However, to verify it, a more precise 3-D model of the building is required.

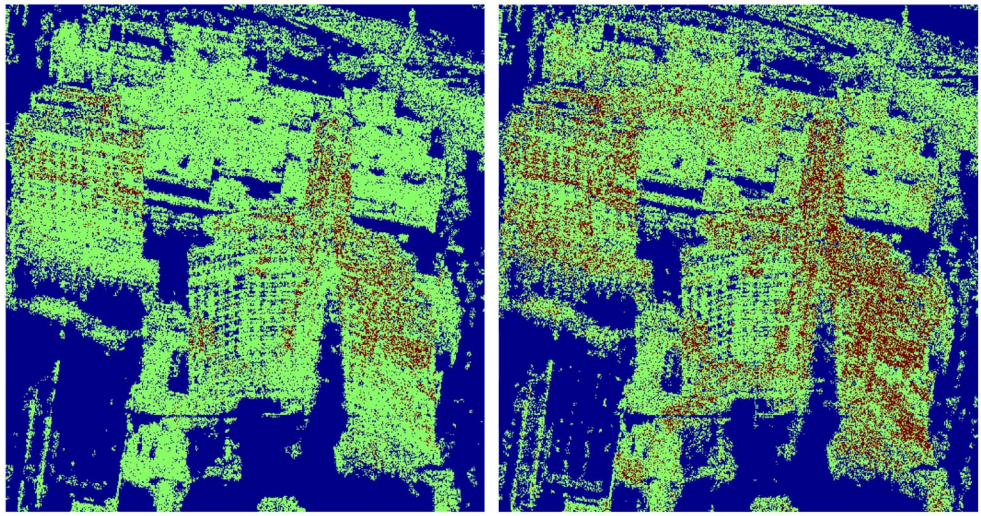

(a) (b)

Fig. 8. Number of scatterers map obtained by MD and SL1MMER at the test area. Blue: zero scatterers inside the azimuth-range pixel; green: one scatterer inside the pixel; red: two scatterers inside the pixels. (a) MD (SVD-Wiener plus model selection). (b) SL1MMER.

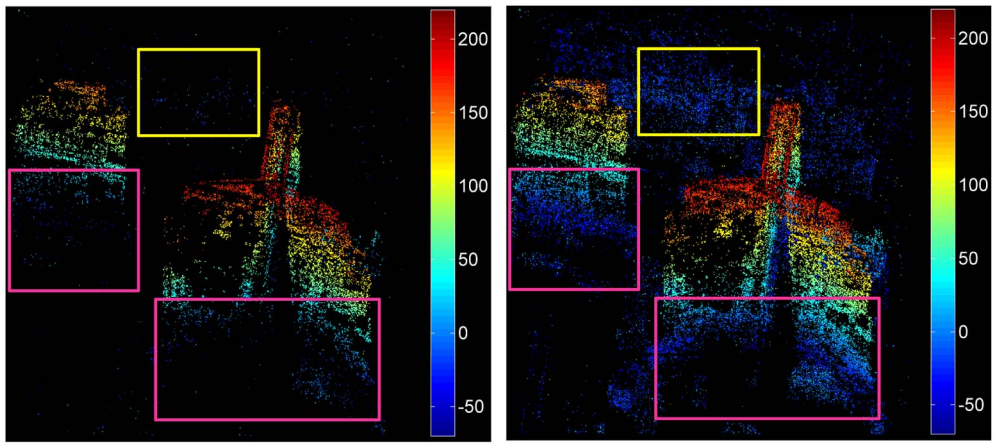

(a) (b)

Fig. 9. MD versus SL1MMER: elevation estimates of the separated double scatterers—one of the two from the building facade. Magenta boxes: areas where the low part of the hotel and the ground structures are mapped together; Yellow box: area where the ground structures (of different height) are mapped together. In both cases, SL1MMER detects a big amount of double scatterers while nonparametric MD cannot well separate them. (a) Building facade: MD. (b) Building facade: SL1MMER.

C. Comparison With Linear Detector: Maxima Detection

In this section, the results obtained by using the SL1MMER algorithm will be compared to the result of maxima detection (MD) [19], i.e., SVD-Wiener (linear MAP) reconstruction followed by peak detection and model order selection and final refinement of the amplitude and phase estimates. For a fair comparison, the later two steps are identical to these in SL1MMER.

Fig. 8 presents the number of scatterers map obtained by MD [Fig. 8(a)] and SL1MMER [Fig. 8(b)] over the test area where blue indicates zero scatterers inside the azimuth-range pixel, green stands for one, and red for two. Linear MAP estimators can only detect two scatterers with an elevation distance larger than approximately the Rayleigh elevation resolution ρ_s (i.e., 40.5 m in elevation, ca. 23.7 m in height). Therefore, it is not surprising that the double scatterers detected by MD are mainly located on the upper part of the building facade. The result of SL1MMER shows a much higher density of detected double scatterers. In the following discussion, the percentage of detected double scatterers is defined with respect to the sum of all detected scatterers, i.e., single plus double (note a pixel including double scatterers is counted twice). For the whole area, 13.1% and 29.9% of the scatterers detected by MD and SL1MMER, respectively, are found as double scatterers. In particular, for an individual building, e.g., the Y-shaped building on the right, SL1MMER increases the percentage of the detected double scatterers from 20.4% (as obtained by MD) to 37.8%. The dramatically improved layover separation capability is mainly associated with the SR power of SL1MMER and is consistent with the theoretical findings of [19]. For example, in Fig. 9, the top layer (building facade) of the double scatterers detected by MD and SL1MMER is illustrated. In addition to the aforementioned information increment within the layover area in general, the marked areas are worthy of special attention. The magenta boxes mark the areas where the lower parts of the hotel facade and the ground structures are mapped together, while the yellow box marks an area where the lower ground

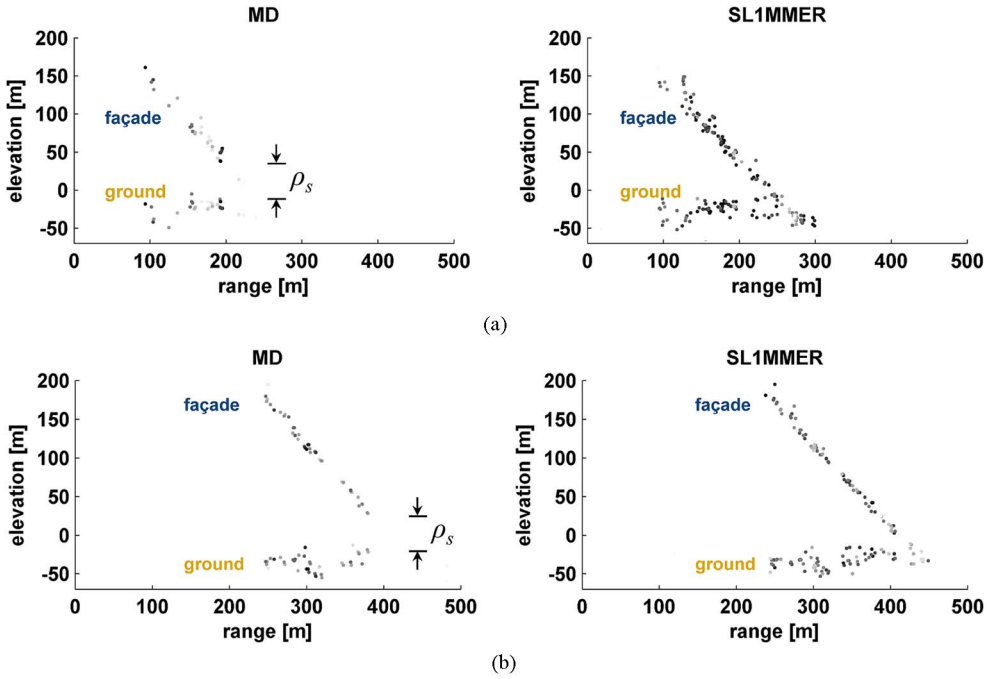

Fig. 10. (Left) MD versus (right) SL1MMER. Reflectivity profiles of the detected double scatterers for slice A and slice B from Fig. 3. The darker the point the stronger the reflection. Note that there is no flat surface in front of the building. (a) Slice A. (b) Slice B.

structures (of different height) are in layover. Those are the typical areas where SR is required for layover separation since the elevation distances between the two scatterers are small. In all marked areas, SL1MMER detects a large amount of double scatterers, while nonparametric MD cannot separate them well which can also be observed in Fig. 8. More obvious evidences can be found in Fig. 10. Two example slices at the positions marked by green arrows in Fig. 3 are chosen as analysis slices. The reflectivity profile in range-elevation plane of the detected double scatterers are extracted using MD (left) and SL1MMER (right). Here, the darker color indicates stronger reflection. Different elevation resolution limits of MD and SL1MMER can be even visually distinguished.

D. Final Evidence

In order to further quantify the SR capability of SL1MMER, the histogram of the elevation distances between each of the detected double scatterer pairs is provided in Fig. 11. As mentioned already, for a fair comparison, we applied the same algorithmic sequence of SL1MMER to the linear reconstruction, i.e., a model selection and a parametric linear least-square estimation of the scatterers' amplitude and phase have been applied after the SVD-Wiener reconstruction. The blue curve represents the result of SL1MMER, while the red curve shows the results of MD. The horizontal axis, i.e., the elevation distance between the detected double scatterers, is normalized to ρ_s. The black line indicates the Rayleigh resolution limit. The case of two scatterers within one Rayleigh resolution cell, i.e., $\alpha = \delta s/\rho_s < 1$, is relevant for SR. In this plot, only on the left-hand side of the black line, the two scatterers are said to be super-resolved.

Fig. 11 demonstrates the following.

- The L_2 norm regularization employed in MD gives also SR though nonsignificant [14].

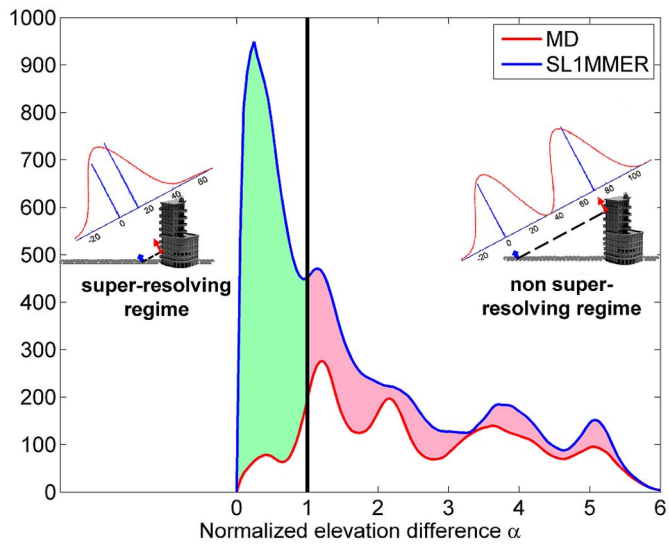

Fig. 11. Histogram of the distance between the detected double scatterers using MD (red) and SL1MMER (blue) (135 bins, distance spacing: 2 m).

- SL1MMER has impressive SR capability, i.e., many of double scatterers with $\alpha < 1$ are detected. In the test area shown in Fig. 3, the SL1MMER algorithm which can provide SR detects 29.9% double scatterers pairs, while 47.1% of them are within the Rayleigh resolution unit. This fact again confirms also the essential role of SR for urban infrastructure mapping.
- The layover separation capability of SL1MMER is much higher compared to MD, i.e., many more double scatterers are detected by SL1MMER than by MD. This superior layover separation capability of SL1MMER is mainly related to SR (green zone). For $\alpha \geq 1$, SL1MMER also provides remarkably better layover separation performance (pink zone). This better performance is mainly caused by the

fact that SL1MMER does not suffer from the interference of the two scatterers (i.e., sidelobes) and has been shown to be more robust against unmodeled phase terms [18].

IV. Conclusion

In this paper, elevation SR is demonstrated to be a crucial requirement for tomographic SAR inversion for urban infrastructure monitoring. Double scatterer pairs with smaller elevation distances are more frequent than those with larger distances.

Experiments using TerraSAR-X data demonstrate that SL1MMER increases significantly the proportion of the detected double scatterers from 20.4% to 37.8%. This almost 100% increase of layover separation capability is proven to be mainly associated with the SR power of SL1MMER. The practical demonstration of SR of SL1MMER presented in this paper completes the methodological investigations in [14], [15], [18], and [19] concerning new tomographic SAR inversion algorithms tailored to very high resolution SAR data.

References

[1] J. Homer, I. Longstaff, and G. Callaghan, "High resolution 3-D SAR via multi-baseline interferometry," in *Proc. IEEE IGARSS*, 1996, vol. 1, pp. 796–798.

[2] P. Pasquali, C. Prati, F. Rocca, M. Seymour, J. Fortuny, E. Ohlmer, and A. Sieber, "A 3-D SAR experiment with EMSL data," in *Proc. IEEE IGARSS*, 10–14, 1995, vol. 1, pp. 784–786.

[3] A. Reigber and A. Moreira, "First demonstration of airborne SAR tomography using multibaseline L-band data," *IEEE Trans. Geosci. Remote Sens.*, vol. 38, no. 5, pp. 2142–2152, Sep. 2000.

[4] F. Lombardini, "Differential tomography: A new framework for SAR interferometry," *IEEE Trans. Geosci. Remote Sens.*, vol. 43, no. 1, pp. 37–44, Jan. 2005.

[5] G. Fornaro, D. Reale, and F. Serafino, "Four-dimensional SAR imaging for height estimation and monitoring of single and double scatterers," *IEEE Trans. Geosci. Remote Sens.*, vol. 47, pt. 2, no. 1, pp. 224–237, Jan. 2009.

[6] X. Zhu, N. Adam, and R. Bamler, "Space-borne high resolution tomographic interferometry," in *Proc. IEEE IGARSS*, 2009, vol. 4, pp. IV-869–IV-872.

[7] D. Reale, G. Fornaro, A. Pauciullo, X. Zhu, and R. Bamler, "Tomographic imaging and monitoring of buildings with very high resolution SAR data," *IEEE Geosci. Remote Sens. Lett.*, vol. 8, no. 4, pp. 661–665, Jul. 2011.

[8] G. Fornaro, F. Lombardini, and F. Serafino, "Three-dimensional multipass SAR focusing: Experiments with long-term spaceborne data," *IEEE Trans. Geosci. Remote Sens.*, vol. 43, no. 4, pp. 702–714, Apr. 2005.

[9] X. Zhu, N. Adam, and R. Bamler, "Space-borne High Resolution SAR Tomography: Experiments in Urban Environment Using TerraSAR-X Data," in *Proc. Urban Remote Sensing Joint event (JURSE)*, Shanghai, China, 2009.

[10] S. Guillaso and A. Reigber, "Scatterer characterisation using polarimetric SAR tomography," in *Proc. IEEE IGARSS*, 2005, vol. 4, pp. 2685–2688.

[11] S. Sauer, L. Ferro-Famil, A. Reigber, and E. Pottier, "Polarimetric dual-baseline InSAR building height estimation at L-band," *IEEE Geosci. Remote Sens. Lett.*, vol. 6, no. 3, pp. 408–412, Jul. 2009.

[12] G. Fornaro and F. Serafino, "Imaging of single and double scatterers in urban areas via SAR tomography," *IEEE Trans. Geosci. Remote Sens.*, vol. 44, no. 12, pp. 3497–3505, Dec. 2006.

[13] A. Ferretti, M. Bianchi, C. Prati, and F. Rocca, "Higher-order permanent scatterers analysis," *EURASIP J. Appl. Signal Process.*, vol. 2005, no. 20, pp. 3231–3242, Jan. 2005.

[14] X. Zhu and R. Bamler, "Very high resolution spaceborne SAR tomography in urban environment," *IEEE Trans. Geosci. Remote Sens.*, vol. 48, no. 12, pp. 4296–4308, Dec. 2010.

[15] X. Zhu and R. Bamler, "Let's do the time warp: Multi-component nonlinear motion estimation in differential SAR tomography," *IEEE Geosci. Remote Sens. Lett.*, vol. 8, no. 4, pp. 735–739, Jul. 2011.

[16] A. Budillon, A. Evangelista, and G. Schirinzi, "SAR tomography from sparse samples," in *Proc. IEEE IGARSS*, 2009, vol. 4, pp. IV-865–IV-868.

[17] X. Zhu and R. Bamler, "Very high resolution SAR tomography via compressive sensing," in *Proc. ESA FRINGE Workshop Adv. Sci. Appl. SAR Interferometry*, Frascati, Italy, 2009.

[18] X. Zhu and R. Bamler, "Tomographic SAR inversion by L_1-norm regularization—The compressive sensing approach," *IEEE Trans. Geosci. Remote Sens.*, vol. 48, no. 10, pp. 3839–3846, Oct. 2010.

[19] X. Zhu and R. Bamler, "Super-resolution power and robustness of compressive sensing for spectral estimation with application to spaceborne tomographic SAR," *IEEE Trans. Geosci. Remote Sens.*, vol. 50, no. 1, pp. 247–258, Jan. 2012.

[20] N. Adam, M. Eineder, N. Yague-Martinez, and R. Bamler, "High resolution interferometric stacking with TerraSAR-X," in *Proc. IEEE IGARSS*, 2008, vol. 2, pp. II-117–II-120.

[21] G. Schwarz, "Estimating the dimension of a model," *Ann. Stat.*, vol. 6, no. 2, pp. 461–464, Mar. 1978.

[22] S. Gernhardt, N. Adam, M. Eineder, and R. Bamler, "Potential of very high resolution SAR for persistent scatterer interferometry in urban areas," *Ann. GIS*, vol. 16, no. 2, pp. 103–111, 2010.

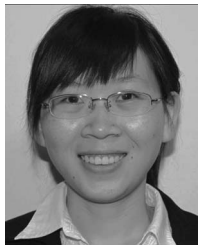

Xiao Xiang Zhu (S'10–M'12) received the Bachelor degree in space engineering from the National University of Defense Technology, Changsha, China, in 2006, and the Master (M.Sc.) and Doctor of Engineering (Dr.-Ing.) degrees from Technische Universität München (TUM), München, Germany, in 2008 and 2011, respectively.

In October/November 2009, she was a Guest Scientist at the Italian National Research Council (CNR)—Institute for Electromagnetic Sensing of the Environment, Naples, Italy. Since May 2011, she has been a full-time scientific collaborator with the Remote Sensing Technology Institute, German Aerospace Center (DLR), Wessling, Germany and with Remote Sensing Technology Department, TUM. Her main research interests are signal processing, including innovative algorithms such as compressive sensing, sparse reconstruction, with applications in the field of remote sensing, in particular 3-D, 4-D, or higher dimensional SAR imaging.

Her Ph.D. dissertation "Very High Resolution Tomographic SAR Inversion for Urban Infrastructure Monitoring—A Sparse and Nonlinear Tour" won the Dimitri N. Chorofas Foundation Research Award in 2011 for its distinguished innovative and sustainability.

Richard Bamler (M'95–SM'00–F'05) received the Diploma degree in electrical engineering, Doctorate degree in engineering, and the "Habilitation" in the field of signal and systems theory from the Technische Universität München (TUM), München, Germany, in 1980, 1986, and 1988, respectively.

He worked at the university from 1981 to 1989 on optical signal processing, holography, wave propagation, and tomography. He joined the German Aerospace Center (DLR), Wessling, Germany, in 1989, where he is currently the Director of the Remote Sensing Technology Institute. In early 1994, he was a Visiting Scientist at the Jet Propulsion Laboratory in preparation for the SIC-C/X-SAR missions, and in 1996, he was Guest Professor at the University of Innsbruck, Innsbruck, Auntria. Since 2003, he has held a full professorship in remote sensing technology at the TUM as a double appointment with his DLR position. His teaching activities include university lectures and courses on signal processing, estimation theory, and SAR. Since 2010, he has been a member of the executive board of Munich Aerospace, a newly founded research and education project between Munich universities and extramural research institutions, including DLR. Since he joined DLR, his team and his institute have been working on SAR and optical remote sensing, image analysis and understanding, stereo reconstruction, computer vision, ocean color, passive and active atmospheric sounding, and laboratory spectrometry. They were and are responsible for the development of the operational processors for SIR-C/X-SAR, SRTM, TerraSAR-X, TanDEM-X, ERS-2/GOME, ENVISAT/SCIAMACHY, MetOp/GOME-2, and EnMAP. He is the author of more than 200 scientific publications, among them 50 journal papers, a book on multidimensional linear systems theory, and holds eight patents and patent applications in remote sensing. His current research interests are in algorithms for optimum information extraction from remote sensing data with emphasis on SAR. This involves new estimation algorithms, like sparse reconstruction and compressive sensing. He has devised several high-precision algorithms for SAR processing, SAR calibration and product validation, GMTI for traffic monitoring, SAR interferometry, phase unwrapping, persistent scatterer interferometry, and differential SAR tomography.